Examination of Ni-based superalloy/intermetallic diffusion couples containing multiphase regions

M.R. McGregor, M. E. Hancock, L. Pallett, W.J. Clegg

June 27, 2019

Abstract

Increasing gas turbine operating temperatures are driving the development of novel coatings for niche applications. One such application is as an anchor phase material for use in the high-pressure turbine stage, for which NiAlTa alloys are a promising candidate. Extended exposure to the high temperatures of this environment can cause interdiffusion of elements between the coating and the underlying blade material. In this study, NiAlTa/CMSX-4 diffusion couples were investigated experimentally and computationally. The couples initially contained two two-phase regions ($\gamma + \gamma'$) and ($\beta + \tau_1$). After heat treatment at 1100 °C, interdiffusion had caused the τ_1 Laves phase in the coating to transform to the τ_2 Heusler phase, and TCP precipitation was observed in the CMSX-4. A CALPHAD-based model, using Thermo-Calc and DICTRA, developed for this system was able to predict the concentration profiles across the diffusion couple at 1000 °C, with the presence of the predicted phases in the interdiffusion zone verified by x-ray diffraction. However, due to the limited diffusion data for intermetallic phases available in the kinetic database, the model predictions were poor at higher temperatures. In order for the development of intermetallic coatings to be aided by CALPHAD-based simulations, more kinetic data is needed for intermetallic phases than is available at present.

Introduction

In a gas turbine engine, leakage of gas from the flow path reduces the efficiency of the engine. This occurs when air escapes over the top of the rotating blades, and therefore does no work [1]. Such losses can be prevented by employing an appropriate sealing method between the stationary casing and the rotating blades.

One such sealing method focusses on achieving sealing by tipping the turbine blades with an abrasive system that cuts a track into surrounding abradable material on the static counterfacing [2]. The abrasive system consists of abrasive particles, usually cubic boron nitride, affixed to the blade tip using a coating known as an anchor phase. This system has to cut effectively, and protect the blade tip from wear to maintain an effective seal. Therefore, the abrasive system is required to remain in place for the lifetime of the engine [3]. Prior research has shown that the currently available anchor phase materials are unable to withstand abrasion at the operating temperatures required for gas turbine engines [4]. The Laves phase strengthened Ni-Al-Ta system has been identified as a possible candidate anchor phase material. This material has been shown to possess sufficient high temperature strength for use in this application [4]. For this investigation a new candidate material, $Ni_{45.3}Al_{44.7}Ta_{10}$, has been chosen. Alloys of this composition contain two phases, β-NiAl and τ_1-NiTaAl [5]. The body centred cubic β phase provides environmental resistance, and the continuous Laves phase, NiTaAl, maintains strength at high temperatures.

CMSX-4 is the superalloy of choice for turbine blades, with a γ/γ' microstructure and a volume fraction of γ' precipitates on the order of 0.7 [6]. When developing a new coating, the compatibility with the underlying superalloy must be considered. This includes considering the thermal expansivity of both materials, and characterising the material interactions that occur when the pair in contact is exposed to operational temperatures. The behaviour of the previous anchor phase candidate, NiCoCrAlY, in contact with the CMSX-4 superalloy, is well understood and known to be not detrimental to the physical properties of the superalloy [7, 8]. It is unknown whether this is the case for the new candidate material $Ni_{45.3}Al_{44.7}Ta_{10}$. It is known to have a similar coefficient of thermal expansion to that of CMSX-4 [4], but how interdiffusion between the CMSX-4 and $Ni_{45.3}Al_{44.7}Ta_{10}$ may affect either material has not been quantified. This may be characterised either through experimental methods, or by use of numerical simulations based on the CALPHAD approach. One such method may be developed using DICTRA, the diffusion module of the well-known CALPHAD programme Thermo-Calc [9]. Ideally, a model could be developed which can make predictions for multiple coating systems, and then only the most promising systems studied experimentally.

Simulations of superalloy/superalloy diffusion couples and superalloy/single-phase diffusion couples have been achieved [10–12], although the process is computationally expensive, due to the nature of the ordering that takes place in γ/γ' systems. Simulating coating systems in contact with superalloys presents an additional challenge as there are often steep diffusion gradients involved, which can be difficult

to simulate in a stable manner [13]. Despite these challenges, there are numerous recent examples in the literature of Thermo-Calc and DICTRA being used to model the behaviour of NiCoCrAlY coatings, due to its important technical applications as a bond coat in thermal barrier coatings [14–16]. As well as modelling interdiffusion between the substrate and coating, some models incorporate the additional effects of surface oxidation [17–19]. Crucially, NiCoCrAlY usually consists only of $\beta + \gamma$ or γ' phases, which have comprehensive thermodynamic and kinetic descriptions in the available Thermo-Calc and DICTRA databases. However, there is little evidence of modelling of entirely intermetallic coatings deposited on superalloys in the literature, especially those based on the Ni-Al-Ta systems, which is likely in part to be due to the limited thermodynamic and kinetic data available. Thermodynamic data for the Ni-Al-Ta systems has been available since an initial assessment in 1991 [20], and the diffusivities in the binary Ni-Al [21, 22] and Ni-Ta [23–25] have been assessed. There have also been recent efforts to characterise diffusivities in the ternary system, although this was limited to low aluminium and tantalum concentrations, and hence only provides characterisation of interdiffusivities in the fcc phase [26]. The mobility of elements within complex intermetallic phases remains uncharacterised, and hence the degree to which this will affect the reliability of any DICTRA based CALPHAD models of intermetallic coatings is unknown. There have been some efforts to use CALPHAD coupled with experiments to guide the design of other NiAl-based materials, in particular those based on the NiAl-Cr and NiAl-Mo systems, which are able to form fibre-reinforced microstructures upon directional solidification [27]. This study use initial CALPHAD predictions to guide alloy design, and the actual results of experiments have not necessarily been reincorporated into the CALPHAD databases.

Therefore, the aim of the presented work is two-fold. Firstly, the authors wished to investigate experimentally the phase formations and compositional evolutions when a $Ni_{45.3}Al_{44.7}Ta_{10}$/CMSX-4 diffusion couple is exposed to high temperatures. Secondly, the authors aimed to develop a DICTRA-based CALPHAD model to predict the microstructural development observed. It is expected that limitations in the available mobility data for intermetallics will lead to deviations between observed and modelled behaviour. However, the extent to which CALPHAD-based diffusion models of intermetallics are limited by this lack of data cannot be known without comparison to experiment. The results of this study add to the call for greater understanding of atomic mobility within intermetallic phases, as without it an entire area of CALPHAD modelling remains of limited use to the intermetallics community.

Experimental

Experimental Methods

Diffusion couple experiments were performed using CMSX-4/$Ni_{45.3}Al_{44.7}Ta_{10}$ diffusion couples. The nominal compositions of the couple end members are given in Table I. $Ni_{45.3}Al_{44.7}Ta_{10}$ was made by

arc-melting (Arc Melter AM, Edmund Buehler) the pure elements (99.99%) in a water-cooled copper hearth, with a non-consumable tungsten electrode to achieve good mixing. Samples were homogenised at 1300 °C for 24 hours and air-cooled. CMSX-4 rods, 9 mm in diameter, were provided by Rolls-Royce plc. The rods and arc-melted bars were cut (Struers Accutom-5, diamond tipped wheel) into sections 10 mm in length. The faces to be bonded were polished to a 1 µm finish using diamond paste. The diffusion couples were produced by bonding one CMSX-4 section and one $Ni_{45.3}Al_{44.7}Ta_{10}$ section together using an induction heated vacuum diffusion bonder. The sections were held at a load of 98.1 N, and heated at a rate of 200 °C min^{-1} to 1000 °C. The sample was held at this temperature for 1 minute, before being allowed to cool in vacuum.

The bonded sample was then cut into 2 mm thick slices, to give 5 samples, manufactured under identical conditions. The slices were sealed in quartz tubes under vacuum, and heat treated for 16 or 100 hours at either 900 °C, 1000 °C or 1100 °C in a box furnace. All quartz tubes were quenched in iced water upon removal from the furnace. Following heat treatment, the diffusion couple slices were ground using progressively finer grades of SiC paper from 600 to 2500 grit for 3 minutes at each stage (Saphir 550, ATM Metallography). They were then ground for 5 minutes using 4000 grit paper before being polished with 1 µm diamond suspension for 3 minutes. The polishing process was completed using 0.06 µm colloidal silica oxide polishing suspension (OPS) diluted with water in a 1:1 ratio for 10 minutes. After OPS polishing, the sample was placed in ethanol and treated in an ultrasonic bath for 10 minutes to remove any remaining colloidal silica.

The polished samples were investigated using scanning electron microscopy (SEM) and electron probe microanalysis (EPMA) on a FEI Nova NanoSEM 450. Samples were imaged in Backscattered Electrion (BSE) mode and line scans were carried out for EPMA analysis (Bruker ESPRIT 1.9) at 15 keV and 221 pA. Analysis of the compositions of the CMSX-4 and $Ni_{45.3}Al_{44.7}Ta_{10}$ was carried out on non-bonded samples from the same bars that were used to prepared diffusion couples. A minimum of 10 spot measurements were used to determine the average alloy composition. These measurements, and the associated error are shown in Table I. Composition profiles for the diffusion couples were obtained perpendicular to the bonding interface across distances of 250 µm or 500 µm, depending on the length of the heat treatment applied.

An automated X-ray diffractometer, Bruker D8 Advance, with a LynxEye EX detector was used with Cu-Kα radiation at 40kV and 40mA to collect X-ray diffraction (XRD) spectra from the bonded and heat-treated samples. X-ray analysis was performed using a fixed divergence slit with a scan rate of 0.35 2θ min^{-1} over a 2θ range of 15-100°.

	$Ni_{45.3}Al_{44.7}Ta_{10}$		CMSX-4		DICTRA input	
	Nominal	Analyzed	Nominal	Analyzed	$Ni_{45.3}Al_{44.7}Ta_{10}$	CMSX-4
Ni	45.3	46.5 ± 1.59	63.75	64.4 ± 2.00	45.294	63.78
Al	44.7	43.6 ± 2.21	12.59	12.2 ± 0.621	44.7	12.59
Ta	10.0	9.91 ± 0.42	2.18	2.25 ± 0.127	10.0	2.18
Cr	-	-	7.58	7.20 ± 0.257	0.001	9.26
Co	-	-	9.26	10.1 ± 0.380	0.001	7.58
Ti	-	-	1.27	1.02 ± 0.085	0.001	0.98
Re	-	-	0.98	0.98 ± 0.087	0.001	1.98
W	-	-	1.98	1.65 ± 0.113	0.001	1.27
Mo	-	-	0.38	0.191 ± 0.0255	0.001	0.38
Hf	-	-	0.03	Not measured	-	-

Table I: Nominal and measured alloy compositions, alongside input for the DICTRA model (atomic fraction).

Diffusion Simulations

The diffusion module of Thermo-Calc, DICTRA, was used to model the CMSX-4/$Ni_{45.3}Al_{44.7}Ta_{10}$ diffusion couples. Thermodynamic and kinetic data were taken from the databases TCNI8 [28] and MOBNI3 [29], respectively. The couple was modelled using the homogenization model [30, 31], which considers the multicomponent, multiphase system as a 1D problem. The partial molar volume of all substitutional elements is assumed to be constant. It is also assumed that the number of vacancies correspond to equilibrium, and formation of pores via vacancy annihilation is not considered. The domain being modelled was discretized into 60 volume elements, the size and position of which were distributed according to two geometric distributions that met in the centre of the simulated volume, to give the highest concentration of volume elements close to the initial interface of the diffusion couple. In each volume element, the local elemental concentrations, temperature and pressure give a resultant local equilibrium which in turn determines the chemical potentials, fractions and composition of the phases present in each volume. This locally minimised Gibbs energy assumption, as opposed to globally minimised Gibbs energy, is a good approximation if the local microstructural length scale is small compared to the long range diffusion distance [30].

The diffusion flux J_k of a species k between two neighbouring volume elements is evaluated in the homogenization model according to [32] as:

$$J_k = -\frac{M_k^{eff} RT}{V_m \Delta z} \sqrt{x_k^{n-1} x_k^n}\; 2\sinh\left(\frac{\Delta \mu_k}{2RT}\right) \tag{1}$$

where M_k^{eff} is the effective mobility of species k, V_m is the molar volume, Δz is the distance between the centres of the two finite volumes considered, x_k^{n-1} and x_k^n denote the mole fractions of species k in neighbouring volumes $n-1$ and n, and $\Delta \mu_k$ is the difference in local chemical potentials between the two finite volumes obtained from the local minimum in Gibbs energy in each volume.

Various methods to evaluate the local kinetic properties exist and are outlined in [30]. Hashin-Shtrikman bounds may not be used in this case due to a lack of diffusion data [13], so in this work the upper Wiener bounds, more generally termed the "Rule of Mixtures", were used to calculate the effective mobilities such that:

$$M_k^{eff} = \sum f^i M_k^i \tag{2}$$

where f^i is the volume fraction of phase i and M_k^i is the mobility of species k in phase i.

All of the simulations modelled a diffusion couple of length 1 mm, with the initial interface at 500 µm. Simulations were performed using the nominal composition of the alloys, due to difficulty obtaining a representative average overall composition for the $Ni_{45.3}Al_{44.7}Ta_{10}$ alloy as the β-NiAl and C14 Laves phases have substantially different compositions. To give the starting compositions shown in Table I the concentrations of each element across the region were defined using an error function expression of the form:

$$c_n = c_1 + \frac{c_2 - c_1}{2}\left[1 + \mathrm{erf}\left(\frac{x - x_i}{s}\right)\right] \tag{3}$$

where c_n is the concentration of element n, c_1 and c_2 are the initial concentrations of the element of each side of the interface, x is the position on the x-axis at which the concentration is being calculated, x_i is the position of the interface between the two materials, given in this case by 500×10^{-6} m, and s is a transition smoothing constant, set to be 5×10^{-7} m. Hf is excluded from the simulation due to its concentration being too low to reliably measure by EPMA for comparison. Very low concentrations of Co, Cr, Re, W, Ti, and Mo are included in the $Ni_{45.3}Al_{44.7}Ta_{10}$ side of the diffusion couple simulation to stabilise the simulation.

Thermo-Calc simulations were carried out to confirm the expected equilibrium phases in the end-member materials of the diffusion couple at the relevant temperatures. Based on this, the four initial phases used in the DICTRA simulation were γ and γ' (equilibrium phases in CMSX-4), and β-NiAl and C14 Laves phase, NiTaAl (equilibrium phases in $Ni_{45.3}Al_{44.7}Ta_{10}$). The additional active phases were the Heusler phase Ni_2TaAl, as well as a selection of detrimental topologically close-packed (TCP) phases that form in CMSX-4 (σ, μ, and P) [33]. Mobility data is only available for three of the initial equilibrium phases, γ, γ', and β-NiAl. Therefore, the Laves phase is treated in calculations as a phase through which no diffusion may occur. A miscibility gap in the μ phase also has to be programmed for manually to allow the simulation to run to completion.

In order to be able to compare experimental composition profiles to calculated composition profiles, 25

line scans were taken for each condition, and the recorded compositions averaged to give an experimental concentration for each element at each grid point. This approach compensates for the large scatter in concentrations in the $Ni_{45.3}Al_{44.7}Ta_{10}$ due to the very low miscibility of tantalum in NiAl. Since the model predicts average bulk composition at any grid point, these calculated experimental values are more comparable than the compositions of any selected individual phase.

Using the centre of volumes defined in the DICTRA simulation as the points of comparison for experimental and calculated data, the error between the concentration profiles may be calculated using least squares error according to Equation 4 [11]:

$$\text{average error} = \left(\frac{1}{n} \sum_{1}^{n} (x_i^{exp} - x_i^{cal})^2 \right)^{\frac{1}{2}} \tag{4}$$

where x_i^{exp} and x_i^{cal} are the experimental and calculated concentration values at the centre of each colume respectively, and n is the number of grid points compared.

The maximum error between the experimental and calculated values for any one elemental concentration profile was the grid point which gave the highest value of $((x_i^{exp} - x_i^{cal})^2)^{1/2}$. Normalized error is calculated according to the method in [11].

Results & Discussion

Diffusion Couple Microstructures

The microstructural changes after heat treatments at 900 °C, 1000 °C and 1100 °C were very similar, with the greatest difference being the extent of interdiffusion between the materials. The changes are most easily seen in the samples treated at 1100 °C, as these had the largest diffusion distance of the samples. Figure 1 shows the development of the diffusion couple microstructure with increasing heat treatment duration at 1100 °C. The cross sections were imaged using back-scattered electrons, so the brightness of a phase is proportional to the average atomic number of said phase. Hence, the β-NiAl appears darkest, C14 NiTaAl and TCP phases appear bright, and the γ and γ' phases fall in between (with a low contrast between γ and γ' due to their similar composition). The bonding process showed no large scale disruptions to the microstructures of the two end-members, and it was verified by EPMA that no significant interdiffusion had occurred. The scale of the Laves phase structure in the $Ni_{45.3}Al_{44.7}Ta_{10}$ is significantly larger than that of the γ' precipitates in the CMSX-4.

Holding at 1100 °C has lead to the development of four distinct regions in the diffusion couple, which may be seen in Figure 1. Far from the interface, the structure of CMSX-4 is unaffected. Close to the interface, an interdiffusion zone (IDZ) has formed in the CMSX-4, similar to that seen when CMSX-4 is aluminised or plat-aluminised [34]. This is a region of β and γ', with brighter TCP phases also

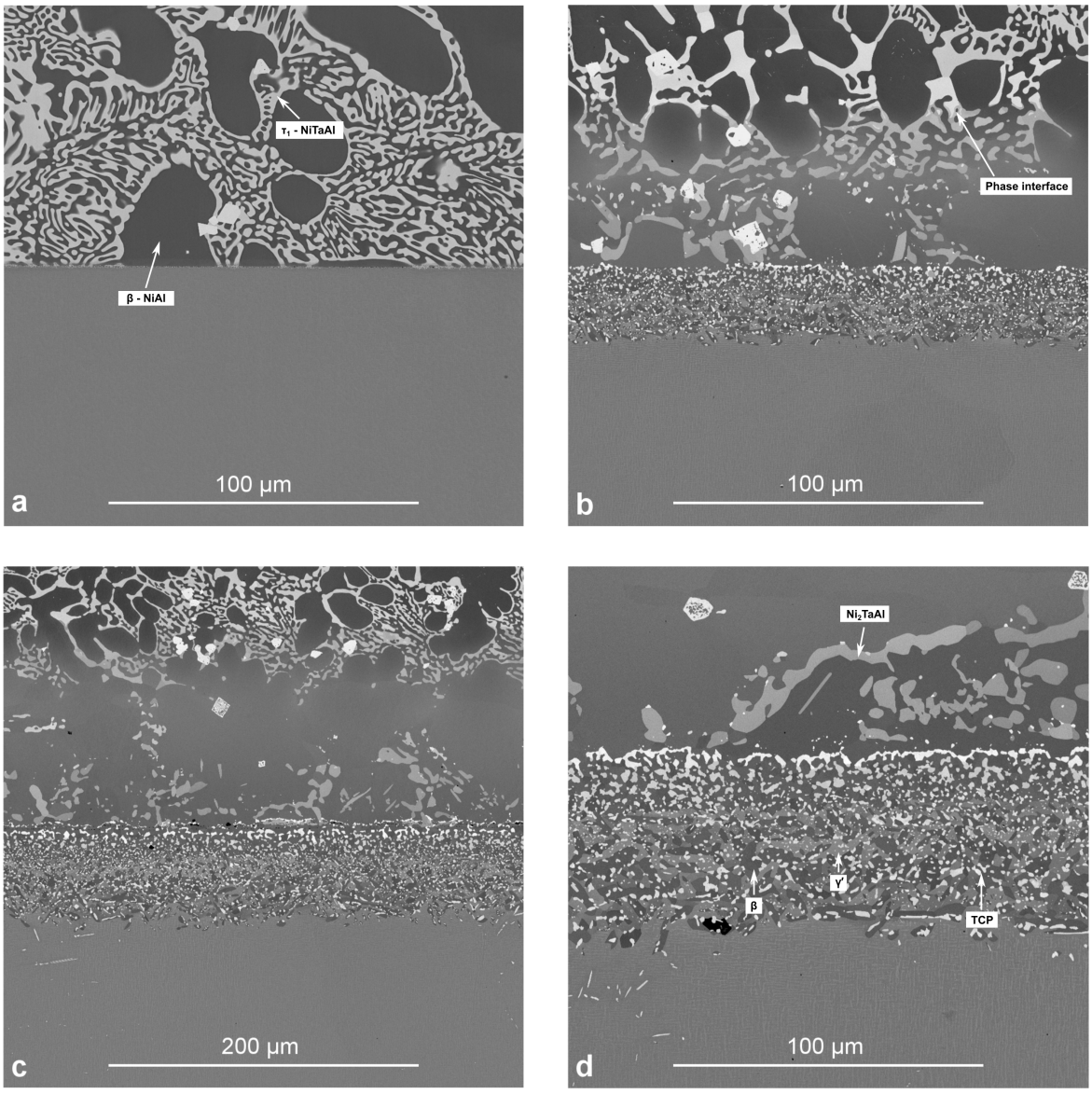

Figure 1: BSE SEM images of the CMSX-4/$Ni_{45.3}Al_{44.7}Ta_{10}$ diffusion couple microstructures (a) as-bonded and after (b) 16 hours and (c) 100 hours at 1100 °C. (d) shows a higher magnification image of the inter-diffusion zone (IDZ) formed in sample (c).

visible. The depth of the IDZ after 100 h at 1100 °C is twice that of the IDZ that forms after 16 h. In the anchor phase side, the BSE reveals that a phase transformation has occured in the coating near the interface. The continuous NiTaAl phase appears to have been partially dissolved. It also shows reduced contrast in BSE mode, indicating a reduction in average atomic number. Far from the interface, the microstructure of the anchor phase remains unchanged. To further characterise the changes taking place during the heat treatment, the EPMA line scans in Figure 2 were collected. These scans show the direction of atomic fluxes for the three component elements of $Ni_{45.3}Al_{44.7}Ta_{10}$. As expected from the concentration gradients present in the initial diffusion couple, nickel diffuses out of the CMSX-4 into the $Ni_{45.3}Al_{44.7}Ta_{10}$, whereas aluminium and tantalum diffuse in the opposite direction from the anchor phase into the superalloy.

Consideration of these fluxes allows for explanation of the observed microstructural regions. The raised nickel concentration in the anchor phase near the interface moves the local alloy composition on the Ni-Ta-Al phase diagram from the β-NiAl + τ_1-NiTaAl two-phase field into the β-NiAl + τ_2-Ni_2AlTa two-phase field [35]. The presence of the Ni_2AlTa Heusler phase was verified using XRD, as shown in Figure 3. Since the continuous nature of the τ_1-NiTaAl Laves phase is responsible for strengthening the material at high temperatures, this transformation to a discontinuous phase is likely to reduce the overall strength of the material [36, 37].

Figure 2 shows that there is an increase in aluminium concentration in the IDZ post heat treatment. This incoming aluminium flux works to stabilise NiAl in the IDZ as can be seen in Figure 1. This phase has a low solid solubility for tantalum, so tantalum is rejected into the surrounding material, contributing to the regions of elevated tantalum content seen in the line scan of the IDZ. Since tantalum is a strong γ' former, this effect in combination with the incoming tantalum flux from the coating stabilises islands of γ'. The increased fraction of γ' causes elements that segregate to the γ, such as rhenium, chromium, molybdenum and tungsten, to quickly super-saturate the remaining γ phase. This leads to the precipitation of TCP phases enriched in these elements in the IDZ. The presence of the TCP phase σ was verified using XRD, with the results shown in Figure 3. The σ (002) peak around 38° has the greatest intensity, potentially due to a texture induced by an orientation relationship with the CMSX-4 [33]. Generally, the σ peak intensity is low, due to a very small crystal size.

The diffusion of tantalum in CMSX-4 may approximated by considering the diffusivity of tantalum in pure nickel, which is given by Equation 5 [23]:

$$D_{Ta}(m^2 s^{-1}) = 2.19 \times 10^{-5} \exp \frac{-251\ kJ\ mol^{-1}}{RT} \tag{5}$$

Substituting Equation 5 into an approximation of Fick's first law, $\bar{x} \approx \sqrt{Dt}$, where $\bar{x}$ is the mean

diffusion distance and t is the time at temperature, tantalum is predicted to diffuse approximately 19 µm after 16 h at 1100 °C and 47 µm after 100 h at 1100 °C. This is comparable to the measured sizes of 24 µm and 55 µm, respectively, suggesting that tantalum diffusion is limiting the size of the IDZ. The overall behaviour of the diffusion couple subjected to heat treatment is summarised in a schematic in Figure 4, showing the zones formed, and the direction of the atomic fluxes.

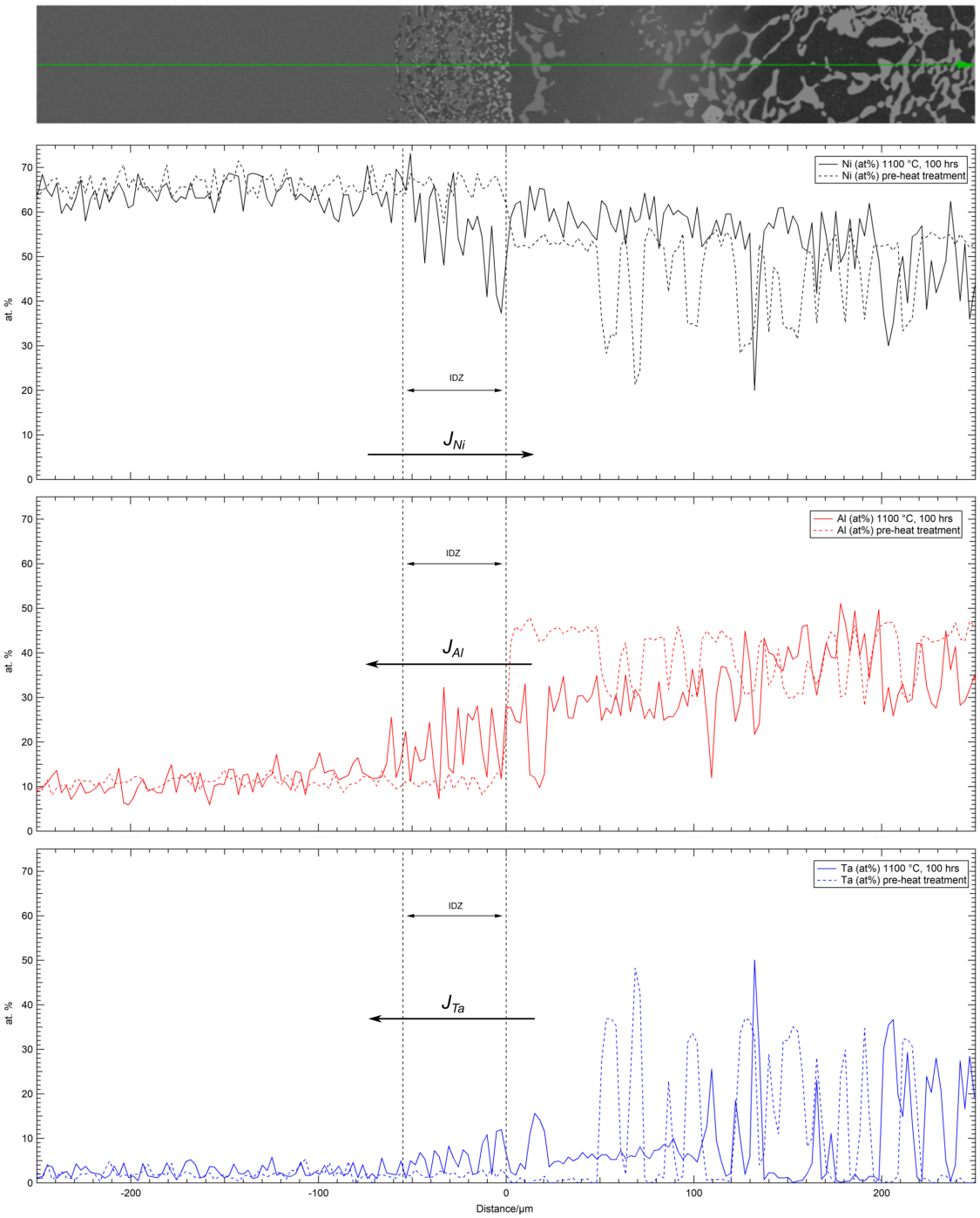

Figure 2: EPMA line scan results from the as-bonded diffusion couple and after 100 h at 1100 °C. Only nickel, tantalum and aluminium are included for clarity.

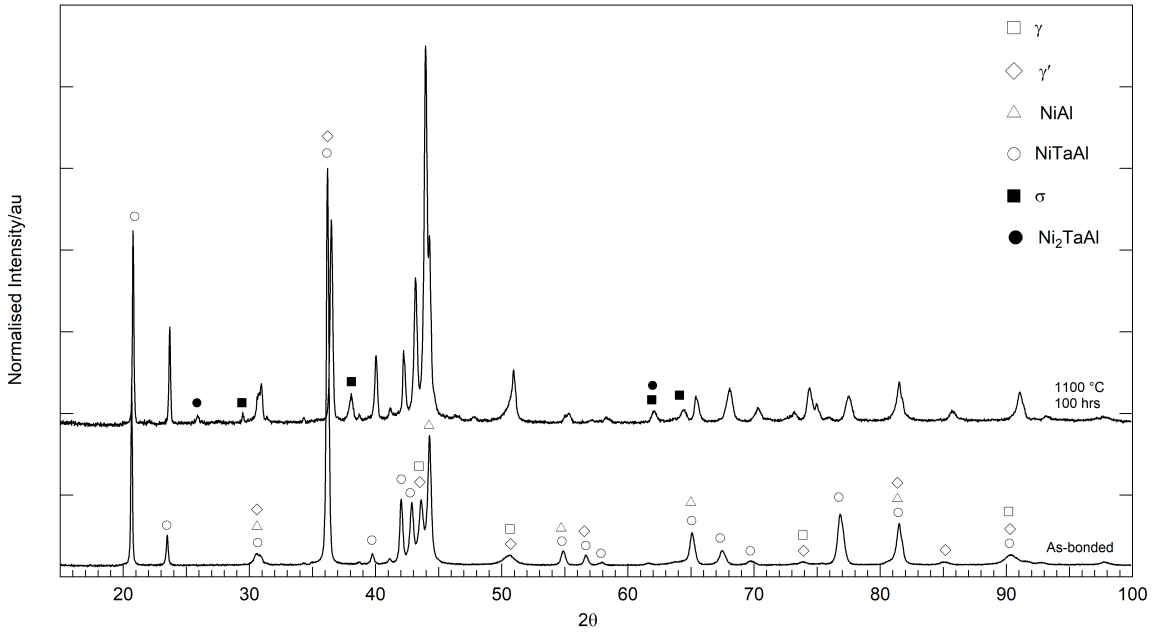

Figure 3: XRD traces for the as-bonded sample and after 100 h at 1100 °C. New peaks in the trace post heat treatment are indicated with filled markers. These new peaks indicate the formation of small amounts of σ and Heusler phase after the diffusion couple has been heat treated.

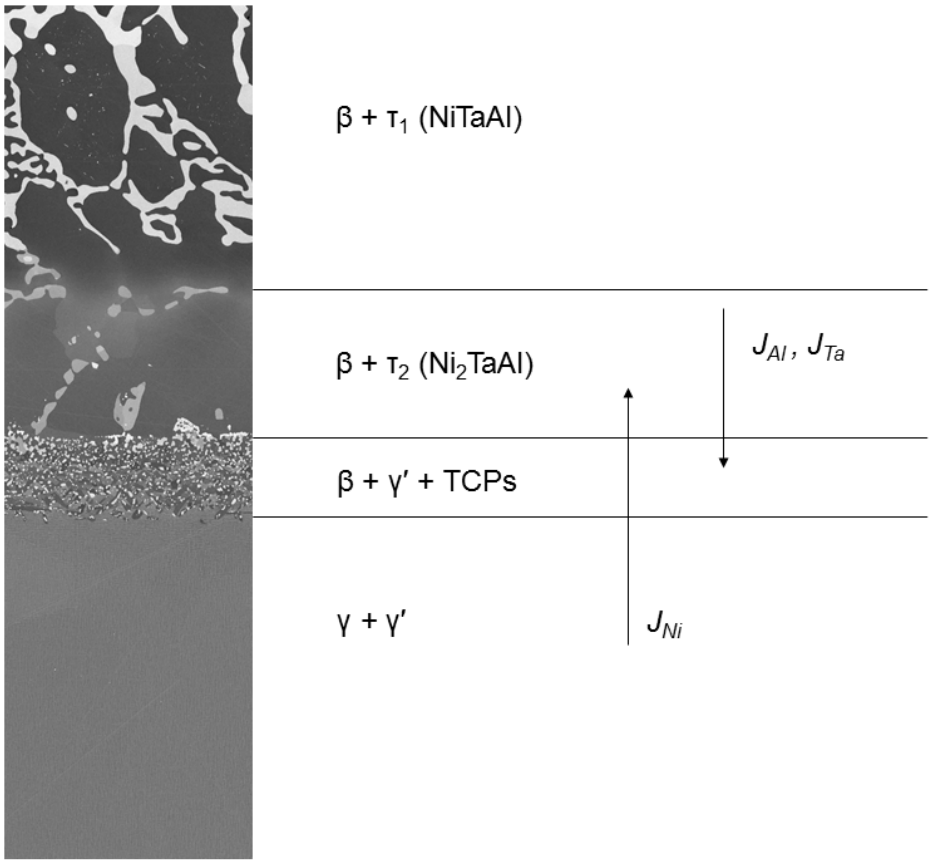

Figure 4: Schematic showing the substrate, coating, inter-diffusion zone (IDZ), and direction of key fluxes between the CMSX-4 and $Ni_{45.3}Al_{44.7}Ta_{10}$ coating.

Simulation Results and Comparisons

Figure 5 compares the measured compositions to the calculated alloy composition profiles for couples treated at a) 1000 °C for 16 h, b) 1100 °C for 16 h and c) 1100 °C for 100 h. In all three cases, the agreement between the simulation and experiment is better for the CMSX-4 side of the diffusion couple than the anchor phase side due in part to the large scatter in experimental reading introduced by the large difference in phase composition between NiAl and NiAlTa. In all three cases, the simulation overestimates the bulk aluminium content of the anchor phase, and correspondingly underestimates the nickel content. This could potentially be due to the averaging factor applied to experimental data, but may also be due to experimental uncertainty in the aluminium EPMA signal.

Of the three simulations, the best agreement is achieved for the 16 h 1000 °C case, as shown in Figure 5a. Here, the overall shape of the predicted diffusion profiles matches well with the experimentally obtained profiles, even though the absolute maximum and minimum values show some error. The extent of interdiffusion into the anchor phase is well predicted, with the experimental diffusion profile levelling off at around 40 µm as predicted. The slight diffusion of both cobalt and chromium observed in the experimental data is also well predicted by the model.

However, when the temperature is raised to 1100 °C, the experimental results and simulation show greater divergence, particularly in the prediction of diffusion into the anchor phase. After 16 h at 1100 °C, the experimental results show that the nickel and aluminium content of the anchor phase have changed up to 75 µm into the anchor phase, whereas the DICTRA model predicts a penetration depth of only around 40 µm, similar to the 1000 °C simulation. However, despite underestimating the extent of diffusion, the simulation predicts the shape of the diffusion profiles in the anchor phase side, with the experimental nickel concentration showing the predicted discontinuous increase in the anchor phase. The measured aluminium concentration also shows the predicted two stage drop-off, although of a significantly larger magnitude than predicted by the simulation. DICTRA struggles to accurately predict the extent of diffusion into and out of the anchor phase for these two elements, because the Heusler phase which is forming cannot be entered in the DICTRA simulation as a phase that facilitates diffusion, due to a lack of kinetic data. This means that the simulation only takes account of diffusion in the bcc NiAl phase, when clearly the dissolution of NiAlTa and formation of Ni_2AlTa plays an important role. However, both the extent of the diffusion of tantalum from the anchor phase into the CMSX-4 and the shape of the resultant concentration profile are well predicted by the simulation, indicating that for the diffusion of tantalum, consideration of the NiAl phase alone is in this case accounting for the dominant diffusion mechanism.

In the 100 h 1100 °C case, the discrepancies between the predicted profiles and the experimental measured ones are greatest, with diffusion affecting the composition up to 200 µm into the anchor phase, and increasing discrepancies in the predicted profile shape. Again, of the three elements making up the

anchor phase, the tantalum predictions best matched the profile observed experimentally, due to the slow diffusing nature of the large tantalum atoms [38]. Experimentally, significant cobalt diffusion into the anchor phase has been measured, but this is not predicted by the simulation.

The conclusions drawn from Figure 5 are complimented by calculating the average error between each calculated and measured profile according to equation 4. Table II shows the maximum, average and normalized errors for each component of the diffusion couples, at the different heat treatment conditions. Errors are quoted in atomic percent. Due to the method used to calculate normalized error (average error divided by average of end member compositions for that element) those elements which are present in CMSX-4 in very small amounts, and not at all in the anchor phase, such as Re, W, Mo and Ti, show very large normalized errors. If the three elements present initially in both systems are considered (nickel, aluminium and tantalum), the error analysis also shows that with increasing heat treatment temperature and time, the accuracy of the DICTRA simulation decreases, with the average error and standard deviation in the error both increasing for these elements across the time and temperature range.

Element	Max error	Average error	σ_{error}	Normalized average error
16 h 1000 °C				
Ni	8.5	3.9	±2.3	7.1
Al	9.6	5.5	±2.9	19.0
Ta	5.3	1.7	±1.7	28.3
Cr	2.8	0.73	±0.72	19.3
Co	2.0	0.91	±0.47	19.7
Ti	0.36	0.20	±0.20	31.8
Mo	0.17	0.08	±0.08	46.8
W	0.86	0.49	±0.41	49.4
Re	1.1	0.64	±0.28	130.9
16 h 1100 °C				
Ni	12.9	4.8	±4.1	8.9
Al	15.7	6.6	±4.9	22.8
Ta	7.2	2.2	±2.1	36.5
Cr	3.7	1.1	±1.1	28.9
Co	4.2	1.4	±1.3	30.8
Ti	0.47	0.23	±0.23	36.9
Mo	0.37	0.10	±0.10	52.9
W	0.73	0.37	±0.29	37.6
Re	0.71	0.41	±0.24	83.7
100 h 1100 °C				
Ni	14.7	6.8	±5.9	12.5
Al	18.9	9.4	±7.1	32.6
Ta	6.0	2.3	±2.2	37.4
Cr	4.7	1.3	±1.3	34.3
Co	5.6	2.1	±1.8	45.4
Ti	0.81	0.26	±0.26	41.0
Mo	0.23	0.08	±0.08	44.4
W	1.3	0.6	±0.37	62.1
Re	1.2	0.70	±0.25	142

Table II: Errors between the measured and predicted profiles in atomic percent.

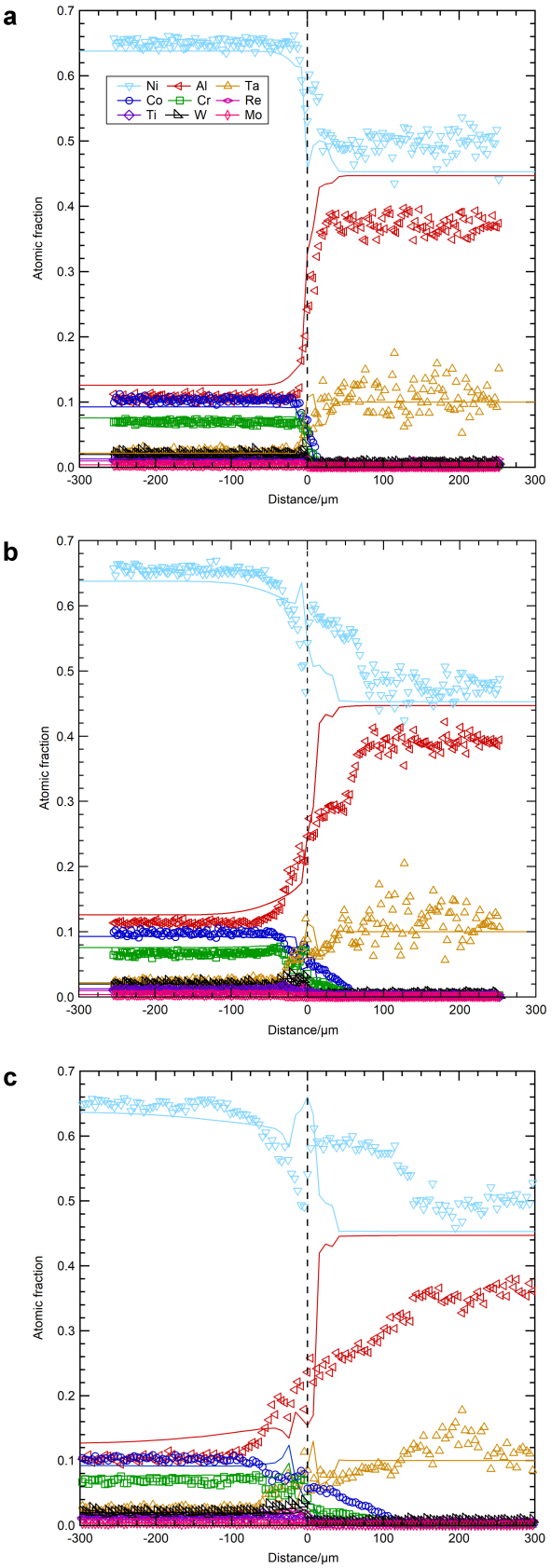

Figure 5: Comparison of measured composition profiles to the overall calculated composition profiles: a) 16 hour 1000 °C, b) 16 hour 1100 °C, c) 100 hour 1100 °C. The measured profiles are denoted using the open markers, and the solid line represents the prediction of the DICTRA model.

Conclusions

Investigation of the interactions of a potential new anchor phase material $Ni_{45.3}Al_{44.7}Ta_{10}$ with the existing blade alloy CMSX-4 was carried out using diffusion couple methods, at a range of temperatures and times. The experimental results were compared with DICTRA simulations of the multiphase diffusion couples. The results of this investigation are as follows:

1. Diffusion of nickel into the anchor phase, and tantalum out of the anchor phase into the CMSX-4 drives the transformation of the reinforcing NiTaAl Laves phase to a discontinuous Ni_2TaAl Heusler phase. This may be detrimental to the abrasion performance of the coating, due to a reduction in strength associated with the transformation.

2. As with aluminised superalloys, diffusion of aluminium into the CMSX-4 stabilises γ' formation in the IDZ, which drives TCP precipitation. This process is accelerated by additional diffusion of tantalum into the CMSX-4 which is a strong γ' former.

3. After heat-treatment at 1000 °C for 16 h, the measured composition profile for tantalum shows agreement with the profile predicted by a multiphase DICTRA simulation. There is some scatter in the experimental measurement due to the large difference in tantalum concentration in the two phases present in the $Ni_{45.3}Al_{44.7}Ta_{10}$. This agreement is despite the lack of mobility data for the τ_1-NiTaAl phase in the initial diffusion couple, or for the Heusler and TCP phases that form during the heat treatment. The shapes of the predicted nickel and aluminium profiles match those of the measured profile, but over-predict and under-predict the concentrations of aluminium and nickel in the $Ni_{45.3}Al_{44.7}Ta_{10}$ respectively. This may be due to the use of nominal composition in the presented DICTRA model.

4. When the temperature is raised to 1100 °C, there is little agreement between the simulation and the experimental data, with the discrepancy increasing with longer heat treatment times. This is due to the lack of mobility data for the initially present τ_1-NiTaAl phase, and for the τ_2-Ni_2TaAl and TCP phases that form during the heat treatment. This highlights the limitations of the currently available Thermo-Calc and DICTRA databases for modelling of this kind of superalloy coating. In order to improve the fit of predicted profiles to experimental data, mobility data is required for more of the intermetallic phases that form in the system, so that the model is more able to capture the nuances of the experimental reality.

Acknowledgements

The authors would like to thank Mrs S. Rhodes and Dr A. Shirzadi for experimental assistance, and Dr R. Thompson for useful comments on the manuscript. This work was supported by the Rolls-Royce/EPSRC

Strategic Partnership under EP/H022309/1 and EP/M005607/1. The underlying experimental data that supports this research is available from: https://doi.org/10.17863/CAM.40214

References

[1] C. Bringhenti and J. R. Barbosa, "Effects of Turbine Tip Clearance of Gas Turbine Performance," in *ASME Turbo Expo 2008: Power for Land, Sea and Air*, pp. 1715–1721, 2008.

[2] S. Gebhard, T. Wobst, D. Roth-Fagaraseanu, and M. Hancock, "Advanced coating systems for future shroudless turbines," in *ASME 2013 Turbine Blade Tip Symposium*, ASME, sep 2013.

[3] Oerlikon Metco, "Improve efficiency and reduce emissions with abradable coatings for steam turbines," 2014.

[4] J. R. Davenport, L. Mendez-Garcia, S. Purkayastha, M. E. Hancock, R. J. Stearn, and W. J. Clegg, "Material needs for turbine sealing at high temperature," *Materials Science and Technology*, vol. 30, no. 15, pp. 1877–1883, 2014.

[5] V. Kuznetsov, "Al-Ni-Ta (Aluminium - Nickel - Tantalum)," in *Light Metal Systems. Part 3*, pp. 1–15, Berlin/Heidelberg: Springer-Verlag, 1991.

[6] A. Sengupta, S. K. Putatunda, L. Bartosiewicz, J. Hangas, P. J. Nailos, M. Peputapeck, and F. E. Alberts, "Tensile behavior of a new single-crystal nickel-based superalloy (CMSX-4) at room and elevated temperatures," *Journal of Materials Engineering and Performance*, vol. 3, no. 1, pp. 73–81, 1994.

[7] J. R. Nicholls, "Advances in Coating Design for High- Performance Gas Turbines," *MRS Bulletin*, no. September, pp. 659–670, 2003.

[8] H. E. Evans and M. P. Taylor, "Diffusion cells and chemical failure of MCrAlY bond coats in thermal-barrier coating systems," *Oxidation of Metals*, vol. 55, no. 12, pp. 17–34, 2001.

[9] A. Borgenstam, A. Engstrom, L. Hoglund, and J. Agren, "DICTRA, a Tool for Simulation of Diffusional Transformations in Alloys," *Journal of Phase Equilibria*, vol. 21, no. 3, pp. 269–280, 2000.

[10] A. Engström, J. Bratberg, Q. Cheng, L. Höglund, and P. K. Mason, "Application of Thermodynamic and Kinetic Modeling to Diffusion Simulations in Nickel-Base Superalloy Systems," *Advanced Materials Research*, vol. 278, pp. 198–203, 2011.

[11] C. E. Campbell, J. C. Zhao, and M. F. Henry, "Examination of Ni-base superalloy diffusion couples containing multiphase regions," *Materials Science and Engineering A*, vol. 407, no. 1-2, pp. 135–146, 2005.

[12] A. Chyrkin, A. Epishin, R. Pillai, T. Link, G. Nolze, and W. J. Quadakkers, "Modeling Interdiffusion Processes in CMSX-10/Ni Diffusion Couple," *Journal of Phase Equilibria and Diffusion*, vol. 37, no. 2, pp. 1–11, 2016.

[13] H. Larsson and L. Höglund, "Multiphase diffusion simulations in 1D using the DICTRA homogenization model," *Calphad: Computer Coupling of Phase Diagrams and Thermochemistry*, vol. 33, no. 3, pp. 495–501, 2009.

[14] A. Forslund and H. Larsson, "Simulation of reaction-diffusion between substrate and coating during vapor deposition processes," *Calphad: Computer Coupling of Phase Diagrams and Thermochemistry*, vol. 64, no. October 2018, pp. 278–283, 2019.

[15] H. Chen and T. Barman, "Thermo-Calc and DICTRA modelling of the β-phase depletion behaviour in CoNiCrAlY coating alloys at different Al contents," *Computational Materials Science*, vol. 147, pp. 103–114, 2018.

[16] T. Galiullin, A. Chyrkin, R. Pillai, R. Vassen, and W. J. Quadakkers, "Effect of alloying elements in Ni-base substrate material on interdiffusion processes in MCrAlY-coated systems," *Surface and Coatings Technology*, vol. 350, no. July, pp. 359–368, 2018.

[17] R. Pillai, W. G. Sloof, A. Chyrkin, L. Singheiser, and W. J. Quadakkers, "A new computational approach for modelling the microstructural evolution and residual lifetime assessment of MCrAlY coatings," *Materials at High Temperatures*, vol. 32, no. 1-2, pp. 57–67, 2015.

[18] R. Pillai, M. P. Taylor, T. Galiullin, A. Chyrkin, E. Wessel, H. Evans, and W. J. Quadakkers, "Predicting the microstructural evolution in a multi-layered corrosion resistant coating on a Ni-base superalloy," *Materials at High Temperatures*, vol. 35, no. 1-3, pp. 78–88, 2018.

[19] R. Pillai, A. Jalowicka, T. Galiullin, D. Naumenko, M. Ernsberger, R. Herzog, and W. J. Quadakkers, "Simulating the effect of aluminizing on a CoNiCrAlY-coated Ni-base superalloy," *Calphad: Computer Coupling of Phase Diagrams and Thermochemistry*, vol. 65, no. January, pp. 340–345, 2019.

[20] L. Kaufman, "Calculation of multicomponent tantalum based phase diagrams," *Calphad*, vol. 15, pp. 261–282, jul 1991.

[21] S. Shankar and L. L. Seigle, "Interdiffusion and Intrinsic Diffusion in the NiAl (delta) Phase of the AI-Ni System," *Metallurgical Transactions A*, vol. 9, no. October, pp. 1467–1476, 1978.

[22] T. Helander and J. Ågren, "Phenomenological treatment of diffusion in Al-Fe and Al-Ni alloys having B2-B.C.C. ordered structure," *Acta Materialia*, vol. 47, no. 4, pp. 1141–1152, 1999.

[23] M. S. A. Karunaratne, P. Carter, and R. C. Reed, "Interdiffusion in the face-centred cubic phase of the Ni–Re, Ni–Ta and Ni–W systems between 900 and 1300 °CC," *Materials Science and Engineering: A*, vol. 281, no. 1–2, pp. 229–233, 2000.

[24] J. Chen, J. Xiao, L. Zhang, and Y. Du, "Interdiffusion in fcc Ni-X (X = Rh, Ta, W, Re and Ir) alloys," *Journal of Alloys and Compounds*, vol. 657, pp. 457–463, 2016.

[25] J. Chen, J. Zhao, L. Zhang, X. G. Lu, and L. Liu, "Atomic mobilities in fcc Ni–rich NiX (X=Rh, Ta, W, Re, and Ir) systems," *Calphad: Computer Coupling of Phase Diagrams and Thermochemistry*, vol. 65, no. March, pp. 316–325, 2019.

[26] J. Chen, L. Zhang, J. Zhong, W. Chen, and Y. Du, "High-throughput measurement of the composition-dependent interdiffusivity matrices in Ni-rich fcc Ni-Al-Ta alloys at elevated temperatures," *Journal of Alloys and Compounds*, vol. 688, pp. 320–328, 2016.

[27] J. Peng, P. Franke, and H. J. Seifert, "Experimental Investigation and CALPHAD Assessment of the Eutectic Trough in the System NiAl-Cr-Mo," *Journal of Phase Equilibria and Diffusion*, vol. 37, no. 5, pp. 592–600, 2016.

[28] "TCNI8 database version 8.1."

[29] "MOBNi3 database version 3.1."

[30] H. Larsson and A. Engström, "A homogenization approach to diffusion simulations applied to $\alpha + \gamma$ Fe-Cr-Ni diffusion couples," *Acta Materialia*, vol. 54, no. 9, pp. 2431–2439, 2006.

[31] H. Larsson, "A model for 1D multiphase moving phase boundary simulations under local equilibrium conditions," *Calphad: Computer Coupling of Phase Diagrams and Thermochemistry*, vol. 47, pp. 1–8, 2014.

[32] H. Larsson, H. Strandlund, and M. Hillert, "Unified treatment of Kirkendall shift and migration of phase interfaces," *Acta Materialia*, vol. 54, no. 4, pp. 945–951, 2006.

[33] C. M. F. Rae and R. C. Reed, "The precipitation of topologically close-packed phases in rhenium-containing superalloys," *Acta Materialia*, vol. 49, no. 19, pp. 4113–4125, 2001.

[34] C. M. F. Rae, M. S. Hook, and R. C. Reed, "The effect of TCP morphology on the development of aluminide coated superalloys," *Materials Science and Engineering A*, vol. 396, no. 1-2, pp. 231–239, 2005.

[35] V. Raghavan, "Al-Ni-Ta (Aluminum-Nickel-Tantalum)," *Journal of Phase Equilibria and Diffusion*, vol. 27, pp. 405–407, aug 2006.

[36] M. Igarashi and H. Senba, "High temperature deformation and oxidation resistance of NiAl based intermetallic compounds," in *International Symposium on Structural Intermetallics* (R. Darolia, J. Lewandowski, C. Liu, P. Martin, D. Miracle, and M. Nathal, eds.), pp. 533–542, The Minerals, Metals and Materials Society, 1993.

[37] B. Zeumer and G. Sauthoff, "Intermetallic NiAl-Ta alloys with strengthening Laves phase for high-temperature applications. I. Basic properties," *Intermetallics*, vol. 5, no. 7, pp. 563–577, 1997.

[38] M. S. A. Karunaratne and R. C. Reed, "Interdiffusion of the platinum-group metals in nickel at elevated temperatures," *Acta Materialia*, vol. 51, no. 10, pp. 2905–2919, 2003.